Thermal Science and Engineering (2023) Volume 6 Issue 1
doi:10.24294/tse.v6i1.2000

ORIGINAL RESEARCH ARTICLE

Towards efficient tandem solar cells based on lead-free and inorganics perovskite absorbers

Hayat Arbouz

Department of Physics, University of Blida 1, Blida 09000, Algeria. E-mail: arbouzhayet@yahoo.fr

ABSTRACT

In this paper, we modeled and simulated two tandem solar cell structures (a) and (b), in a two-terminal configuration based on inorganic and lead-free absorber materials. The structures are composed of sub-cells already studied in our previous work, where we simulated the impact of defect density and recombination rate at the interfaces, as well as that of the thicknesses of the charge transport and absorber layers, on the photovoltaic performance. We also studied the performance resulting from the use of different materials for the electron and hole transport layers. The two structures studied include a bottom cell based on the perovskite material $CsSnI_3$ with a band gap energy of 1.3 eV and a thickness of 1.5 µm. The first structure has an upper sub-cell based on the $CsSnGeI_3$ material with an energy of 1.5 eV, while the second has an upper sub-cell made of Cs_2TiBr_6 with a band gap energy of 1.6 eV. The theoretical model used to evaluate the photocurrent density, current-voltage characteristic, and photovoltaic parameters of the constituent sub-cells and the tandem device was described. Current matching analysis was performed to find the ideal combination of absorber thicknesses that allows the same current density to be shared. An efficiency of 29.8% was obtained with a short circuit current density J_{sc} = 19.92 mA/cm^2, an open circuit potential V_{oc} = 1.46 V and a form factor FF = 91.5% with the first structure (a), for a top absorber thickness of $CsSnGeI_3$ of 190 nm, while an efficiency of 26.8% with J_{sc} = 16.74, V_{oc} = 1.50 V and FF = 91.4% was obtained with the second structure (b), for a top absorber thickness of Cs_2TiBr_6 of 300 nm. The objective of this study is to develop efficient, low-cost, stable and non-toxic tandem devices based on lead-free and inorganic perovskite.

Keywords: Perovskite; Solar Cell; Photovoltaics; Tandem; Organic-inorganic

ARTICLE INFO

Received: 28 March 2023
Accepted: 22 May 2023
Available online: 4 June 2023

1. Introduction

The containment period during the COVID-19 pandemic demonstrated the need to preserve the environment and showed the fragility of the oil and gas industry[1]. After the recovery from the pandemic, studies have shown the increase in demand for renewable energy that surged after containment, especially for solar energy[2].

The transition to renewable energies could improve the life of humans while preserving the environment in addition to meeting the great demand for energy that life on earth requires in all its forms. Solar photovoltaic energy seems to meet all these criteria and stands out from other renewable energy sources. However, the cost of solar energy is much higher than conventional sources. Therefore, manufacturing low-cost, high-efficiency devices is essential to lower the cost of solar energy. Silicon-based solar cells have dominated the market[3]; the record efficiency of the cells is just over 26%. Perovskites have emerged as promising materials. Halogenated perovskite PSC solar cells are expected to significantly improve the photovoltaic industry due to their low production cost,

outstanding efficiency and remarkable properties[4], such as tunable band gap in the range of 1.1 eV to 2.3 eV, high electron mobility of about 5–10 $cm^2 V^{-1} s^{-1}$ and high hole mobility of 1–5 $cm^2 V^{-1} s^{-1}$ in addition to high carrier lifetime of 1 µs. The power conversion efficiency of Perovskite organic-inorganic hybrid single junction solar cells OIHPSCs has increased rapidly from 3.8% to 25.2% in just one decade[5]. The organic-inorganic lead halide Perovskites, such as $MAPbI_3$ and $FAPbI_3$, follow the typical stoichiometry ABX_3, where, (A) represents the organic part which is either, made of Methylammonium (MA) or Formamidinium (FA). It may also be non-organic such as Cesium. (B) is usually lead or one of its non-toxic substitutes. (X) represents a halide such as iodine, bromine or chlorine. The world's highest power conversion efficiency for a perovskite solar cell is 25.8%[6]. However, the most performing perovskite solar cells are lead-based, and consequently highly toxic. This is why several studies have undertaken the development of lead-free perovskite-based solar cells, where lead was replaced by tin, germanium, bismuth, antimony and other substances. Many experimental and simulation works in this context have been reported[7]. The goal of most of these studies is to match the performance of their lead-based counterparts.

In any case, whether it is a perovskite-based cell with or without lead, as is the case for all single-junction solar cells, the Schokley-Keisser limit due to thermalization losses[8] has never been reached.

It is therefore essential to move towards tandem structures that can potentially exceed this limit by combining materials with different bandgaps, for better exploitation of the solar spectrum.

Given their tailored band gaps, perovskite semiconductors can provide narrow-band absorbers between 1 eV and 1.4 eV and wide-band absorbers between 1.6 eV and 1.9 eV, simply by varying the composition[9], which makes them excellent candidates for narrow and wide bandgap absorbing materials in tandem and multi-junction structures. In addition, perovskite materials can be deposited using relatively simple fabrication methods. Several tandem structures based on perovskites in combination with Silicon or CIGS materials as narrow absorbers have been reported[10,11].

In this paper, we have modeled, simulated and optimized two different tandem solar cell structures, in which both parts are single cells based on lead-free perovskite materials with appropriate band gaps. In both proposed structures, the narrow bandgap absorber in the bottom part is the tin-based perovskite $CsSnI_3$, with a bandgap of 1.3 eV. In the first structure, the top cell absorber is the tin-germanium based $CsSnGeI_3$ perovskite, with a band gap of 1.5 eV, while in the second structure, the lead-free Cs_2TiBr_6 double perovskite, with 1.6 eV is used as the top absorber. A two-terminal monolithic configuration was considered in both structures with a single interconnection, to minimize spectral losses and reduce manufacturing costs.

All selected sub-cells, both top and bottom, have already been studied in our previous work, where the absorber thickness and bulk defect density have been optimized, and proper selection of electron and hole charge transport layers aimed at minimizing the interface recombination rate has been achieved[12,13]. Since a two-terminal tandem configuration was considered in which the subcells are connected in series, the current matching analysis was performed by varying the thickness of the top absorber to find the same current density flowing through the entire device, so as to reduce current losses.

The objective is to develop and optimize, structures of tandem solar cells, based on inorganic and lead-free absorber materials, with optimal thicknesses, which can be realized using low-cost processes, with or without encapsulation.

2. Methodology of the work

First, the two-terminal tandem (2T-Tandem) configuration was chosen because it requires only one interconnect layer to connect the subcells and is more efficient than the four-terminal tandem configuration.

We opted for absorbers of perovskite which have revolutionized the world of photovoltaics with their properties, rapid development and high efficiency, and have also demonstrated their effectiveness in a single configuration.

Non-organic lead-free absorbers were considered in the proposed structures (a) and (b), because of their non-toxicity, ease of manufacture, and superior stability to their pure lead counterparts.

The two simulated structures (a) and (b) have the same bottom sub-cell based on the narrow bandgap perovskite $CsSnI_3$, but have different upper sub-cells of wide bandgap perovskites, $CsSnGeI_3$ and Cs_2TiBr_6.

The lower and upper perovskite subcells used in the studied tandem structures have been the subject of previous work. The optimization of these subcells focused on the thickness of the absorber and charge transport layers, the density of bulk defects, the state of the interfaces, and finally the choice of ETL and HTL materials with appropriate electronic parameters and that respect the optimal values of the bandgap shifts.

An appropriate model, described below, was used for the simulation. The results obtained were discussed and compared with other similar studies in the literature.

3. Device structure

The two simulated devices (a) and (b) are connected in 2T tandem and composed of the lower subcell based on the $CsInS_3$ perovskite absorber with a bandgap energy of 1.3 eV and a thickness of 1.5 µm, optimized in our previous work, which follows the configuration: FTO/SnO_2/$CsSnI_3$/Spiro-OMeTAD, where SnO_2 and Spiro-OMeTAD are the electron and hole charge transport layers ETL and HTL, respectively. An FTO-fluorotin oxide layer is used as the transparent conductive oxide layer in the bottom subcell. This layer also serves as an interconnect layer between the two parts of the tandem device because it represents an excellent ohmic contact. In the first structure (a), the single perovskite cell based on $CsSnGeI_3$ with 1.5 eV sandwiched between the ETL-PCBM and HTL-Spiro-OMeTAD charge transport layers was used as the top sub-cell. In the second structure (b), the single cell based on the Cs_2TiBr_6 dual perovskite material with a bandgap energy of 1.6 eV was used as the top subcell, configured: SnO_2/Cs_2TiBr_6/NiO, where SnO_2 and NiO represent ETL and HTL, respectively. All of these subcells were optimized in previous work.

Figure 1 shows a schematic representation of the two simulated tandem solar cells (a) and (b), in which the optimal thicknesses of the absorbers, ETL and HTL layers are shown. It is important to note that in addition to their non-toxicity, the perovskite absorber materials studied in these structures are completely inorganic and thus more stable than their organic counterparts $MAPbI_3$ and $FAPbI_3$.

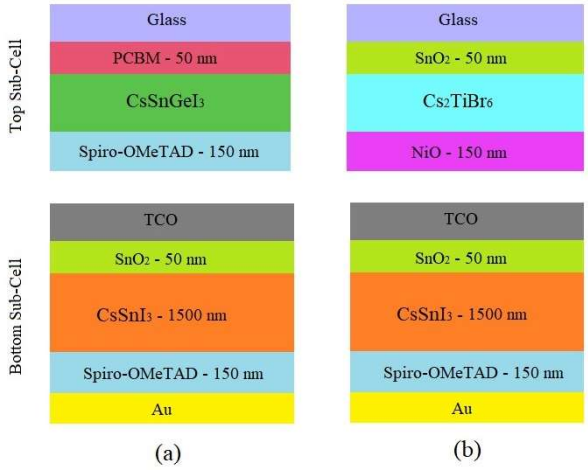

Figure 1. Schematic representation of the simulated structures (a) and (b).

4. Theoretical model

The continuity equations and Poisson's equation are the basis of establishing the physical devices model[14] that allow to calculate the total photocurrent density as a function of the wavelength[15].

The incident light is usually modeled by the AM 1.5 G spectrum. However, in order to facilitate the calculations, Equation (1), which represents a very close approximation of the AM 1.5 G spectrum, was used.

$$IRS(\lambda) = 0.006977 + 7.0625\left[1 - e\frac{-(\lambda - 0.2605)}{0.15994}\right]^{2.28411} \cdot e\frac{-(\lambda - 0.2605)}{0.22285} \quad (1)$$

Since the cell is top-illuminated, the top sub-cell directly receives the solar spectrum described in this work by $IRS(\lambda)$. The incident light passes through all the layers of the upper sub-cell, therefore, the lower part of the tandem device will receive a filtered

spectrum[16] which is calculated according to the following Equation (2).

$$S_{flitered}(\lambda) = IRS(\lambda).exp[-\sum_{i} \alpha_{Top,i}(\lambda).d_i] \quad (2)$$

$\alpha_{Top,i}(\lambda)$ is the coefficient of absorption of the each considered layer i of the top sub-cell, which was calculated using the model of Tauc[17], as expressed in Equation (3), and d_i is the corresponding thickness.

$$\alpha(\lambda) = A.(\frac{hc}{\lambda} - E_g)^{1/2} \quad (3)$$

A is a wavelength-independent constant, and E_g is the energy of the bandgap.

The photo generated current density of top and bottom sub-cells were calculated using Equations (4) and (5).

$$J_{ph,Top} = q.\int_{\lambda_{min}}^{\lambda_{max}} .\frac{\lambda}{hc}.IRS(\lambda).EQE_{top}(\lambda)d\lambda \quad (4)$$

$$J_{ph,Bot} = q.\int_{\lambda_{min}}^{\lambda_{max}} .\frac{\lambda}{hc}.S_{filtered}(\lambda).EQE_{bot}(\lambda)d\lambda \quad (5)$$

where, $EQE_{top,bot}(\lambda)$ is the external quantum efficiency of top and bottom sub-cells, λ_{min} and λ_{max} are minimum and maximum wavelengths and q is the electron charge, h is the constant of Planck and c is the speed of light.

The density of defects of the absorber layer was evaluated according to the Schockley-Read-Hall recombination model, the expression of the recombination rate is as mentioned in Equation (6).

$$R_{SRH} = \frac{n.p - n_i^2}{\tau_p.(n + n_i) + \tau_p.(p + p_i)} \quad (6)$$

where, n and p are the concentrations of elctrons and holes respectivrly, while τ_n and τ_p are carrier lifetimes, calculated by (7).

$$\tau_{n,p} = \frac{1}{\sigma_{n,p}.V_{th}.N_t} \quad (7)$$

N_t is the defect density in the perovskite material, V_{th} is the thermal velocity and $\sigma_{n,p}$ is the electron, hole capture cross section.

A two diodes equivalent circuit was considered to model the dependence of the total density of current generated by each sub-cell, on the applied voltage V and the temperature of the cell T, in realistic conditions, including series and shunt parasitic resistances R_s and R_{sh}[18].

$$J = J_{ph} - (J_0 + J_s).(e^{\frac{q.(V-JR_s)}{2k}} - 1) - \frac{V - J.R_S}{R_{sh}} \quad (8)$$

where, J_{ph} represents the total photogenerated current density, J_0 is the recombination reverse dark current density due to the radiative recombination from the space charge region expressed in Equation (9) as function of diffusion coefficients D_n and D_p, and donor and acceptor carrier densities N_A and N_D. J_s is the interface recombination contribution in current losses due to the presence of density of traps at front and rear interfaces[19], which depends on interface recombination velocity S, given by Equation (10) and conduction and valence energy bandgap offsets at interfaces, ΔE_c and ΔE_v expressed underneath by Equations (11) and (12).

$$J_0 = q.(\frac{\sqrt{D_p}}{\sqrt{\tau_p}}.\frac{n_i^2}{N_D} + \frac{\sqrt{D_n}}{\sqrt{\tau_n}}.\frac{n_i^2}{N_A}) \quad (9)$$

$$S = V_{th}.\sigma.N_{int} \quad (10)$$

N_{th} is the interfacial defect density and σ is the capture cross section of traps.

$$\Delta E_c = \chi_{ETL} - \chi_{Abs} \quad (11)$$

$$\Delta E_v = (\chi_{HTL} + Eg_{HTL}) - (\chi_{Abs} + Eg_{Abs}) \quad (12)$$

The fill factor y of each part of the device was calculated using the formula reported by Cao *et al*.[20]. While the power conversion efficiency was evaluated by the well-known Equation (13).

$$\eta = \frac{J_{sc}.V_{oc}}{P_i} \quad (13)$$

J_{sc}, V_{oc} and P_i are the short current density, the open circuit voltage and the incident power given by Equation (14), respectively.

$$P_i = \int_{\lambda_{min}}^{\lambda_{max}} IRS(\lambda)d\lambda \quad (14)$$

The open circuit voltage of a tandem cell is the sum of the individual open circuit voltages of the top and bottom cells. In contrast, the total current density

is limited to the lowest value provided by the sub-cells[21].

The parameters of all the materials used in the different layers of the studied structures have been carefully selected from experimental and simulation works available in the literature[22,23].

The photovoltaic performance of the optimal $CsSnI_3$, $CsSnGeI_3$, and Cs_2TiBr_6 based single cells that are used as sub-cells in the tandem structures presented in this work are grouped in **Table 1**. These results are compared to similar simulation work based on the same perovskite absorbers[24–26].

5. Results and discussion

Table 1. Performance of the studied single cells

Single cell	E_g (eV)	J_{ph} (mA/cm^2)	V_{oc} (V)	FF (%)	PCE (%)
$CsSnI_3$	1.3	32.21	0.831	74.24	21.23
$CsSnI_3$[24]	1.3	29.67	0.970	70.00	20.29
$CsSnGeI_3$	1.5	27.40	0.830	74.36	18.06
$CsSnGeI_3$[25]	1.5	24.79	1.000	80.71	22.15
Cs_2TiBr_6	1.6	19.06	0.837	84.73	13.90
Cs_2TiBr_6[26]	1.6	25.82	1.100	51.70	14.68

A difference in results, although not significant, is noted between ours and those reported, this is due to the difference in the simulation model, charge transport layer materials and absorber thicknesses.

The corresponding current-voltage curves are plotted in **Figure 2**.

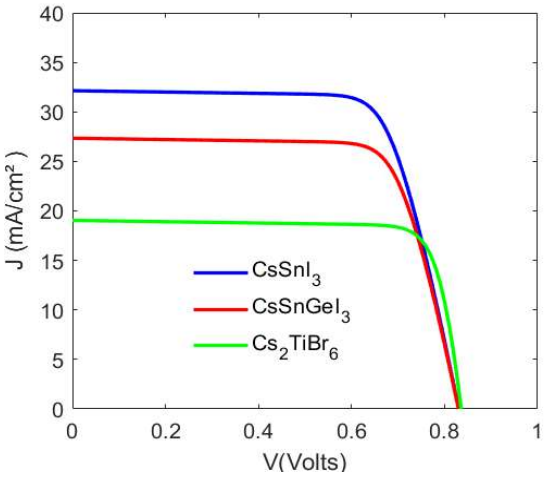

Figure 2. J-V characteristics of the studied single cells.

The bandgap energy of the upper sub-cell is larger and absorbs the short wavelengths of the solar spectrum, while the absorber of the lower sub-cell, which has narrower bandgap energy, absorbs the short wavelengths. On the other hand, since the two sub-cells are monolithically deposited and connected in series, the current density is limited to the lower current density, resulting in high current loss. It is therefore essential that the same current flows through both sub-cells in operation. This is called the current matching condition, which is achieved by adjusting the thickness of the absorbers in an appropriate ratio to find the current matching point.

The second part of this study consists in performing the current matching analysis, for this purpose, the thickness of the lower absorber was set to 1.5 µm for which the $CsSnI_3$-based cell achieved the best conversion efficiency, while the thickness of the upper absorber was varied from 100 nm to 400 nm as shown in **Figure 3** and **Figure 4**.

Figure 3 shows that increasing the thickness of the upper $CsSnGeI_3$ absorber allows light tuning between the upper and lower sub-cells and results in an increase in the current density of the upper sub-cell, but a decrease in that of the lower cell. This current matching occurs in the first tandem structure (a) at a top cell $CsSnGeI_3$ absorber thickness of w = 190 nm, at which both subcells share the same current density of 19.92 mA/cm². **Figure 4** shows that 300 nm is the thickness at which the current matching condition happened, where the sub-cells of Cs_2TiBr_6 and $CsSnI_3$ share the current density value of 16.74 mA/cm². In addition, it is important to note that by reducing the thickness of the upper absorber, the entire device will be thinner.

The obtained photovoltaic parameters of the tandem cell structures are shown in **Table 2** and compared with the performance of similar tandem cells reported in literature.

The results of the photovoltaic parameters of structures (a) and (b) are presented in **Table 2**.

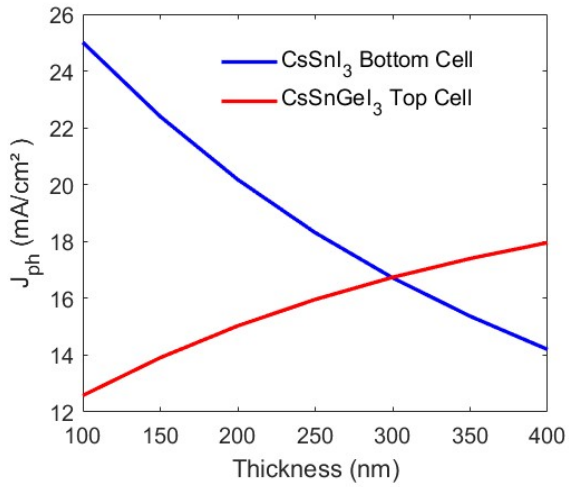

Figure 3. Current matching analysis in 2T-$CsSnGeI_3$/$CsSnI_3$ tandem solar cell: Structure (a).

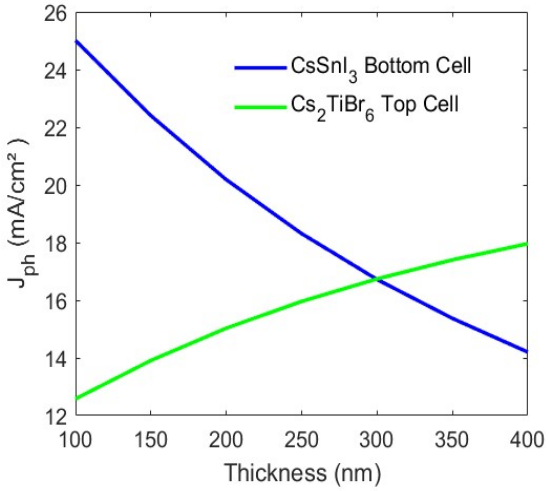

Figure 4. Current matching analysis in 2T-Cs_2TiBr_6/$CsSnI_3$ tandem solar cell: Structure (b).

Table 2. Performance of the simulated tandem cells

Tandem cell	w_{Bot} (nm)	w_{Top} (nm)	J_{ph} (mA/cm^2)	V_{oc} (V)	FF (%)	PCE (%)
$CsSnGeI_3$/$CsSnI_3$	1,500	190	19.92	1.462	91.5	29.67
Cs_2TiBr_6/$CsSnI_3$	1,500	300	16.74	1.501	91.4	26.79
$CsSnGeI_3$/$CsSnI_3$[27]	815	450	21.22	1.210	71.32	18.32
$Cs_2AgBiSbBr_6$/FACsP-$bSnI_3$[28]	400	380	14.90	1.832	63.57	17.35
Lead-based[29]	1,150	350	15.5	2.012	79.3	24.7
$MAPbI_3$/Si[30]	4.10^5	187.9	16.3	/	/	31.4

Based on the obtained values, it can be seen that each structure has advantages and disadvantages. Structure (a), whose top absorber is $CsSnGeI_3$, achieved an efficiency of more than 29% with a top absorber thickness of only 190 nm. However, although this absorber is completely inorganic, the surrounding ETL and HTL charge transport layers of PCBM and Spiro-OMeTAD respectively are organics. Not to mention the HTL layer of Spiro-ometad in the lower sub-cell.

This is likely to increase the instability of the device. Structure (b), with Cs_2TiBr_6 as the top absorber, achieved an efficiency of more than 26%, lower than that of the first structure and with a 300 nm thicker top absorber. However, except for the HTL layer of the lower subcell, all other layers are inorganic, which is an advantage for the stability of the device. There remains the problem of the instability of the lower $CsSnI_3$ absorber due to the presence of tin which tends to oxidize and cause degradation of the device. In this case, encapsulation is strongly recommended. Both structures are completely lead-free and contain no other toxic elements, making them environmentally friendly devices.

Compared to the results of $CsSnGeI_3$/$CsSnI_3$[27] and $Cs_2AgBiSbBr_6$/$FACsPbSnI_3$[28] devices mentioned in **Table 2**, the combination of absorber thicknesses allowing current matching is more optimal than that of our work, but the photovoltaic performance is lower. In addition, the structure based on the lower subcell of $FACsPbSnI_3$ and that reported in reference[29] contain lead unlike ours. We have also reported the performance of the MAPbI3/Si tandem structure[30] which achieved an efficiency of more than 31%. However, in addition to the lead in the upper absorber, the lower subcell is silicon-based and very thick.

The current-voltage curves of the two simulated tandem structures (a) and (b) are illustrated in **Figure 5**.

After this research, we are able to propose structure (a) as the optimal structure for a stable and non-toxic lead-free and inorganics perovskites-based 2T-tandem device. It is important to note that all layers included in the structure can be deposited by simple and inexpensive processes.

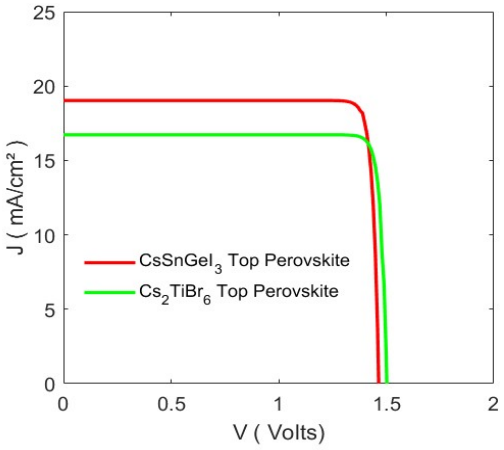

Figure 5. J-V curves of the simulated tandem structures.

6. Conclusion

In this study, two-terminal tandem perovskite solar cell structures based on lead-free absorbers were modeled and simulated. In both proposed structures, all constituent sub-cells are non-toxic. The absorbers are lead-free and inorganic. In both structures (a) and (b), the bottom sub-cell is based on $CsSnI_3$ perovskite that contains tin instead of lead, with a band gap of 1.3 eV. In structure (a), the absorber of the upper cell is $CsSnGeI_3$ perovskite based on the tin-germanium mixture with a band gap of 1.5 eV, while in the second structure (b), the absorber is based on lead-free Cs_2TiBr_6 double perovskite with a band gap of 1.6 eV. All selected sub-cells were previously optimized with respect to constituent layer thicknesses, bulk and interface defect densities, and the selection of electron and hole charge transport layers. A suitable simulation model to calculate the photo-current density, the J-V curve of each sub-cell and the photovoltaic parameters of the tandem solar cell have been described. The current matching analysis was performed by varying the thickness of the top absorber to match the photo-current and reduce the thickness of the top sub-cell. An efficiency of 26.8% was obtained with the first structure (a) for 190 nm thickness of the top absorber $CsSnGeI_3$, and 29.7% with the second structure (b) for 300 nm thickness of the top absorber Cs_2TiBr_6. The results were compared with similar devices reported in the literature. Our research suggested that the structure (a) is an efficient and optimal 2T-Tandem solar cell device based on inorganic and lead-free absorbers, which is non-toxic, relatively stable and low cost. This study could be very informative before proceeding to the fabrication stage.

Conflict of interest

The author declares no conflict of interest.

References

1. Petroleum Economist. COVID-19 puts African energy on pause [Internet]. London: Petroleum Economist; 2020. Available from: https://pemedianetwork.com/petroleum-economist/articles/upstream/2020/covid-19-puts-african-energy-on-pause/.
2. Hoang AT, Nižetić S, Olcer AI, *et al*. Impacts of COVID-19 pandemic on the global energy system and the shift progress to renewable energy: Opportunities challenges and policy implications. Energy Policy 2021; 154: 112322. doi: 10.1016/j.enpol.2021.112322.
3. Richter A, Müller R, Benick J, *et al*. Design rules for high-efficiency both-sides-contacted silicon solar cells with balanced charge carrier transport and recombination losses. Nature Energy 2021; 6(4): 429–438. doi: 10.1038/s41560-021-00805-w.
4. You P, Tang G, Yan F. Two-dimensional materials in perovskite solar cells. Materials Today Energy 2019; 11: 128–158. doi: 10.1016/j.mtener.2018.11.006.
5. Tong G, Ono LK, Qi Y. Recent progress of all bromide inorganic perovskite solar cells. Energy Technology 2019; 8(4): 1900961. doi: 10.1002/ente.201900961.
6. Wang S, Wang A, Hao F. Toward stable lead halide perovskite solar cells: A knob on the A/X sites components. iScience 2022; 25(1): 103599. doi: 10.1016/j.isci.2021.103599.
7. Li J, Duan J, Yang X, *et al*. Review on recent progress of lead-free halide perovskites in optoelectronic applications. Nano Energy 2021; 80: 105526. doi: 10.1016/j.nanoen.2020.105526.
8. Wang K, Zheng L, Hou Y, *et al*. Overcoming Shockley-Queisser limit using halide perovskite platform. Joule 2022; 6(4): 756–771. doi: 10.1016/j.joule.2022.01.009.
9. Chen Q, Marco ND, Yang Y, *et al*. Under the spotlight: The organic-inorganic hybrid halide perovskite for optoelectronic applications. Nano Today 2015; 10(3): 355–396. doi: 10.1016/j.nantod.2015.04.009.
10. Duan L, Walter D, Chang N, *et al*. Stability challenges for the commercialization of perovskite—Silicon tandem solar cells. Nature Reviews Materials 2023; 8: 261–281. doi: 10.1038/s41578-022-00521-1.
11. Jošt M, Köhnen E, Al-Ashouri A, *et al*. Perovskite/CIGS tandem solar cells: From certified

24.2% toward 30% and beyond. ACS Energy Letters 2022; 7(4): 1298–1307. doi: 10.1021/acsenergylett.2c00274.
12. Arbouz H. Optimization of lead-free $CsSnI_3$-based perovskite solar cell structure. Applied Rheology 2023; 33(1): 20220138. doi: 10.1515/arh-2022-0138.
13. Arbouz H. Simulation and optimization of a lead-free CS_2TiBr_6 perovskite solar cell structure. In: Proceedings of International Conference on Electrical Computer Communications and Mechatronics Engineering; 2022 Nov 16–18; Malé. New York: IEEE; 2022. p. 1–6.
14. Li D, Song L, Chen Y, *et al*. Modeling thin film solar cells: From organic to perovskite. Advanced Science 2019; 7(1): 1901397. doi: 10.1002/advs.201901397.
15. Sam R, Diasso A, Zouma B, Zougmoré F. 2D modeling of solar cell p-n radial junction: Study of photocurrent density and quantum efficiency in static mode under monochromatic illumination. Smart Grid and Renewable Energy 2020; 11(12): 191–200. doi: 10.4236/sgre.2020.1112012.
16. Kumar A, Singh S, Mohammed MK, Shalan AE. Computational modelling of two terminal CIGS/Perovskite tandem solar cells with power conversion efficiency of 23.1%. European Journal of Inorganic Chemistry 2021; 2021(47): 4959–4969. doi: 10.1002/ejic.202100214.
17. Viezbicke BD, Patel S, Davis BE, Birnie III DP. Evaluation of the Tauc method for optical absorption edge determination: ZnO thin films as a model system. Physica Status Solidi B 2015; 252(8): 1700–1710. doi: 10.1002/pssb.201552007.
18. Courel M, Andrade-Arvizu JA, Vigil-Galán O. Towards a CdS/Cu_2ZnSnS_4 solar cell efficiency improvement: A theoretical approach. Applied Physics Letters 2014; 105(23): 233501. doi: 10.1063/1.4903826.
19. Hermerschmidt F, Savva A, Georgiou E, *et al*. Influence of the hole transporting layer on the thermal stability of inverted organic photovoltaics using accelerated-heat lifetime protocols. ACS Applied Materials and Interfaces 2017; 9(16): 14136–14144. doi: 10.1021/acsami.7b01183.
20. Cao Q, Li Y, Zhang H, *et al*. Efficient and stable inverted perovskite solar cells with very high fill factors via incorporation of star-shaped polymer. Science Advances 2021; 7(28). doi: 10.1126/sciadv.abg0633.
21. Arbouz H. Modeling of a tandem solar cell structure based on CZTS and CZTSe absorber materials. International Journal of Computational Science and Engineering 2022; 8(1): 14–18. doi: 10.22399/ijcesen.843038.
22. Bansal S, Aryal P. Evaluation of new materials for electron and hole transport layers in perovskite-based solar cells through SCAPS-1D simulations. In: Proceedings of the 43rd Photovoltaic Specialists Conference (PVSC); 2016 Jun 5–10; Portland. New York: IEEE; 2016. p. 0747–0750.
23. Jani MR, Islam MT, Al Amin SM, *et al*. Exploring solar cell performance of inorganic Cs_2TiBr_6 halide double perovskite: A numerical study. Superlattices and Microstructures 2020; 146: 106652. doi: 10.1016/j.spmi.2020.106652.
24. Lin S, Zhang B, Lü TY, *et al*. Inorganic lead-free B-γ-$CsSnI_3$ perovskite solar cells using diverse electron-transporting materials: A simulation study. ACS Omega 2021; 6(40): 26689–26698. doi: 10.1021/acsomega.1c04096.
25. Singh N, Agarwal A, Agarwal M. Numerical simulation of highly efficient lead-free perovskite layers for the application of all-perovskite multi-junction solar cell. Superlattices and Microstructures 2021; 149: 106750. doi: 10.1016/j.spmi.2020.106750.
26. Moiz SA. Optimization of hole and electron transport layer for highly efficient lead-free Cs_2TiBr_6-based perovskite solar cell. Photonics 2022*;* 9(1): 23. doi: 10.3390/photonics9010023.
27. Islam MT, Jani MR, Rahman S, *et al*. Investigation of non-Pb all-perovskite 4-T mechanically stacked and 2-T monolithic tandem solar devices utilizing SCAPS simulation. SN Applied Sciences 2021; 3: 504. doi: 10.1007/s42452-021-04487-7.
28. Madan J, Shivani, Pandey R, Sharma R. Device simulation of 17.3% efficient lead-free all-perovskite tandem solar cell. Solar Energy 2020; 197: 212–221. doi: 10.1016/j.solener.2020.01.006.
29. Kumar A, Singh S, Mohammed MKA, Shalan AE. Computational modelling of two terminal CIGS/perovskite tandem solar cells with power conversion efficiency of 23.1%. European Journal of Inorganic Chemistry 2021; 47: 4959–4969. doi: 10.1002/ejic.202100214.
30. Xiao K, Lin R, Han Q. *et al.* All-perovskite tandem solar cells with 24.2% certified efficiency and area over 1 cm using surface-anchoring zwitterionic antioxidant. Nature Energy 2020; 5: 870–880. doi: 10.1038/s41560-020-00705-5.